Bell 412 modeling and model fidelity assessment for level-d training simulators

Myrand-Lapierre, Vincent; Tischler, Mark B.; Pavel, Marilena D.; Nadeau-Beaulieu, Michel; Stroosma, Olaf; Gubbels, Bill; White, Mark

Publication date
2020

Document Version
Final published version

Citation (APA)
Myrand-Lapierre, V., Tischler, M. B., Pavel, M. D., Nadeau-Beaulieu, M., Stroosma, O., Gubbels, B., & White, M. (2020). *Bell 412 modeling and model fidelity assessment for level-d training simulators*. Paper presented at Vertical Flight Society's 76th Annual Forum and Technology Display, Virtual, Online.

Important note
To cite this publication, please use the final published version (if applicable).
Please check the document version above.

Bell 412 Modeling and Model Fidelity Assessment for Level-D Training Simulators

Vincent Myrand-Lapierre
Subject Matter Expert
CAE, Global Engineering
St-Laurent, Québec, Canada

Mark B. Tischler
Senior Technologist
TDD, CCDC Aviation & Missile Center
Moffett Field, CA, US

Marilena D. Pavel
Associate Professor
Delft University of Technology
The Netherlands

Michel Nadeau-Beaulieu
System/Software Developer
CAE, Global Engineering
St-Laurent, Québec, Canada

Olaf Stroosma
Researcher Flight Simulation
Delft University of Technology,
The Netherlands

Bill Gubbels
Principal Research
Officer NRC, Flight
Research Laboratory,
Ottawa, Ontario, Canada

Mark White
Senior Lecturer
School of Engineering,
The University of Liverpool,
Liverpool, UK

ABSTRACT

This paper presents the validation of a Level-D rotorcraft simulation framework by comparing different quantitative model fidelity metrics. The simulation framework uses a non-linear blade element rotor model to simulate the flight dynamics of rotorcrafts with accurate stability and control characteristics identified from system identification techniques. For this study, frequency-domain system identification is used to generate linear state-space 6-DoF quasi-steady models and an automated process is used to adjust the non-linear simulation framework. Regulatory authorities assess performance models for Level-D simulators by comparing time-domain simulation responses with measured aircraft responses for the same set of control inputs. Over the years, new quantitative fidelity metrics were proposed, like the Maximum Unnoticeable Added Dynamics and the Allowable Error Envelopes. This paper will focus on the blade element rotor model hover modeling process to demonstrate its application using a Bell 412 flight test data package. It will also show how this modeling approach can be used to match both Level-D requirements and the alternative fidelity metrics stated above.

NOTATION

Symbols

a_x, a_y, a_z	body-fixed linear accelerometers, ft/s^2 or m/s^2
g	acceleration of gravity, ft/s^2 or m/s^2
g_i^s	identified control derivatives *i* value
g_i^M	calculated control derivatives *i* value
J	cost function
L, M, N	moment derivatives
X, Y, Z	force derivatives
p, q, r	roll, pitch, and yaw rate, rad/s or deg/s
u, v, w	body-fixed velocity components, ft/s
w_i	weighting factor
$\delta_{lon}, \delta_{lat}$	longitudinal and lateral cyclic control input, %
$\delta_{col}, \delta_{ped}$	collective and pedal control input, %
e_β	flap hinge offset, %
δ_3	rotor blade pitch-flap coupling angle, deg
Φ	combination of design variables
$\Delta\theta_1$	swashplate phase angle offset, deg
ϕ, θ, ψ	roll, pitch, and yaw angle, rad or deg
τ	time delay, s
$(\ )_0$	trim point
ω	frequency, rad/s

Abbreviation

AEE	Allowable Error Envelops
CG	Center of Gravity
CR	Cramer-Rao Bound
DoF	Degrees of Freedom
F/M	Force and Moment
MUAD	Maximum Unnoticeable Added Dynamics
OO-BERM	Object Oriented Blade Element Rotor Model
SME	Subject Matter Expert
QTG	Qualification Test Guide
NRC	National Research Council

INTRODUCTION

Helicopter training simulators need to provide high-fidelity immersive environments for pilots in order to obtain

Presented at the Vertical Flight Society's 76th Annual Forum & Technology Display, Virginia Beach, Virginia, USA, Oct. 6-8, 2020.

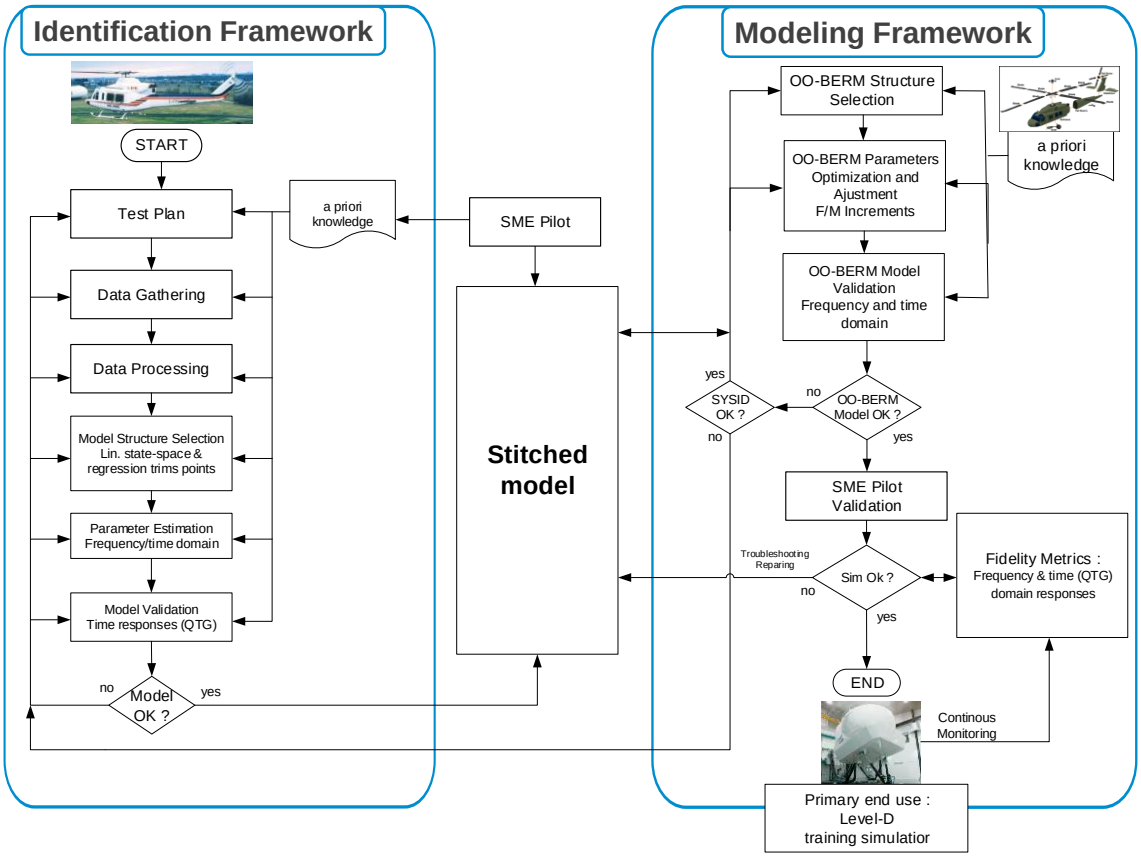

Figure 1 CAE rotorcraft modeling framework for Level-D training simulators

a Level-D qualification, which is the highest level of simulator qualification defined by the Federal Aviation Administration (FAA) [1] and the European Aviation Safety Agency (EASA) [2]. A Level-D qualification allows the replacement of most of the flight hours required for a pilot's type rating or recurrent training by simulator hours. A Level D simulator is made of many sub-system models related to the vehicle dynamics (flight dynamics, flight controls, engines, autopilot), vehicles systems (avionics, ancillaries, etc.) and simulator immersive cueing environments (motion, sound, visual, weather, airport environment, etc.). Each of these sub-systems must meet qualitative and quantitative validation criteria for the specific aircraft type to meet Level-D simulator requirements. This paper will concentrate on the flight dynamics model sub-system which is currently validated by comparing simulated aircraft response time histories with the flight test data for a set of required maneuvers to ensure simulation is within the Level-D imposed tolerances.

CAE is a global leader in training for the civil aviation, defence and security, and healthcare markets. CAE has been developing rotorcraft flight dynamics models from flight test data for more than 20 years [3-7]. Currently, CAE uses a real-time nonlinear simulation platform called "Object Oriented Blade Element Rotor Model" (OO-BERM) [6]. The OO-BERM is a flight mechanics simulation framework that allows users to compose multibody vehicle models of scalable fidelity at simulation load time using C++ compiled libraries. In the last years [7], CAE has developed a systematic method to develop a high-fidelity model for Level-D pilot helicopter training simulation. Those methods are used to develop latest CAE 3000 and 700MR Series military helicopter flight and mission simulators (e.g. Airbus H135/145, Bell 412EP/429, Eurocopter AS365, Sikorsky S-92/UH60-M).

NATO AVT-296 is a 3-year research working group on "Rotorcraft Flight Simulation Model Fidelity Improvement and Assessment". This working group has 3 main objectives. The first objective is to collect and evaluate fidelity assessment methods and metrics. The second objective is to develop and document various methods (simple to more complex) for updating rotorcraft flight dynamics math models for different applications (engineering simulators, training simulator devices, etc.) using flight test data. Finally, the working group will provide lessons learned and best practices for fidelity assessment and improvement. The working group participants represent 17 organizations from 9 NATO countries. The effort will be followed by a short course offered at several NATO locations in 2021 to present and disseminate key findings of the effort. Seven (7) methods of developing and updating aerodynamic models are analyzed within this workgroup (see Table 1). The primary applicability of this paper is to end use training simulators, hence three (3) methods are used. The first one, "Force and Moment (F/M) Increments Based on Stability Derivatives" (Method 3), refers to correcting deficiencies (model compared to flight test data) with incremental forces and moments as 'delta' derivatives. The second method,

"Simulation Model Parameter Adjustment" (Method 5), refers to updating physics-based models with influence from well-established theoretical physical relationships of uncertain parameters. Finally, "Stitched Simulation from Point ID Models and Trim Data" (Method 7), refers to a complete replacement of the physics-based model with a full flight envelope stitched model developed for different flight operating points that makes direct use of the system identification models and trim data.

Table 1 Model Fidelity Improvement Methods

Method	
1	Gain/Time Delay Corrections for Key Responses
2	"Black Box" Lower-Order Transfer-Functions Corrections
3	Force and Moment Increments Based on Stability Derivatives
4	Reduced Order Models and Physics-Based Corrections
5	Simulation Model Parameter Adjustment
6	Parameter Identification of Key Simulation Constants
7	Stitched Simulation from Point ID Models and Trim Data

System identification methods and their application are widely used for helicopter modeling and simulation [9-11]. In [8, 12], system identification methods and tools were compared by different organizations within the NATO AVT-296 working group using a common Bell 412 flight test database provided by the National Research Council (NRC) [15].

CAE's rotorcraft modeling framework (Figure 1) can be separated in two parts, corresponding to the major steps required for model development identification framework and modeling framework. Using flight test data, stability and control behavior are estimated in the identification framework using a combination of frequency- and time-domain based identification methodologies to generate state-space models. Control derivatives and dynamic stability derivatives are identified from dynamic maneuvers of inputs from each helicopter control performed at different initial flight conditions. Linear and non-linear static stability derivatives are identified from a database of many static trim points covering the complete flight envelope, including gross weight/CG combinations, low speed azimuths, autorotation and turns. The system identification framework can integrate methods to estimate parameters that are widely used, like the output-error maximum likelihood method in the frequency domain [11] and the CIFER® frequency response method [9]. The latter is used for this case study. Speed-stability constraint equations can also be implemented within the identification framework.

All estimated parameters are integrated into a stitched model architecture database [19], where a linear interpolation is usually used between the identified trim points. Subject Matter Expert (SME) pilot can also fill the gap in the database when flight test data is missing or when subjective correction are required for the core and edge of the flight envelope. The stitched model is used only for development and validation purpose by the developers. The end-goal is to "mirror" this complete stitched model into the OO-BERM.

First, a Baseline OO-BERM model is set-up to simulate a certain type of helicopter. Using data and measurement available, several parameters are fixed in the simulation like the main rotor configuration, flight control gearing (blade angles [deg] vs control inputs [%]) and aerodynamics surfaces and positions. Then, an optimization framework is used to adjust unknown aeromechanical parameters (e.g. rotor blade pitch-flap coupling angle) in the OO-BERM to best match trim model operation points in the stitched model database. The specific optimization objective is to minimize the residuals between flight test identified control derivatives and control derivatives obtained by linearization of the OO-BERM using numerical approximation. Manual tuning of these unknown aeromechanical parameters is possible, but it is extremely time consuming and may not lead to the best overall set of parameters. Once the solution has been validated and the optimal solution is within reasonable values, force and moment increments are calculated using the dynamic and stability target derivatives to complete the updated OO-BERM model (Method 3, Table 1). Those increments are calculated for a pre-defined helicopter configuration for an extended full flight envelope (maximum rearward/sideward speeds up to VNE, in ground effect (IGE), climb/descent/autorotation and turns). In addition to using dynamic time series validation maneuvers from a trim condition, frequency responses of each input-output relationship are calculated. The choice to sufficiently excite each input-output relationship technique is left to the model developer, as this depends on the simulation framework and tools available. Frequency response matrix calculation is performed by solving a simple system of linear equations over a wide range of frequencies.

The paper will present the different steps leading to a Level-D physics-based model in hover. First, the database (Bell 412) is described. Parameter estimation of the hover rolling and pitching model only is presented and results output from the OO-BERM modeling framework (Baseline and Updated model) are shown. Validation is done in the frequency and time domain. Finally, alternative metrics assessment is presented.

DATABASE

The case study in this paper is based on the Bell 412 ASRA airborne research simulator [15] (Figure 2). The Bell 412 ASRA is derived from the Bell 412HP (high performance) helicopter and is a medium, twin powerplant helicopter with a maximum take-off weight of 11,900 lbs, powered by a PT6T-3BE twin-pac turboshaft engine, rated at 1800 SHP (shaft horse power). This aircraft has a 4-bladed soft-in-plane rotor system featuring high control power and

low response time delays. Installed in the ASRA is an experimental, single string fly-by-wire control system used for research purposes.

Figure 2. NRC Bell 412 ASRA

The database consists of test points flown in a wide variety of steady state conditions throughout the aircraft's flight envelope, as well as dynamic maneuvers in the low speed regime. Test points include hover, forward flight to VNE, climbs, descents, autorotative descents, coordinated turns up to 45 degrees of bank, steady side slips and a selection of ADS-33 maneuvers. Additionally, a set of aircraft modelling data suitable for use in system identification was collected. This included frequency sweeps and 2-3-1-1 maneuvers in hover and at 30, 60, 90 and 120 knots. Also collected were 2-3-1-1's in climbs and descents.

Table 2. Available aircraft modeling data

Data Type	Details
Configuration Data	Main rotor cyclic blade angle ranges Main rotor collective blade angle ranges Tail rotor collective blade angle ranges Tail rotor delta-3 Main rotor mass and stiffness data Horizontal stabilizer dimensions and airfoil Horizontal stabilizer spring properties (stab is spring loaded) Vertical stabilizer dimensions and airfoil Main rotor 3-D scanned model (step file) Fuselage 3-D scanned model (step file)
Flight Test Data	Trim points hover, 30, 60, 90, 120 kts Climbs and descents at 60, 75, 90, 105 kts and with 500, 1000, 1500, 2000 ft/min Runs up & down the runway at 5, 10, 15, 20, 25, 30 kts at 30 degree azimuths Beta sweeps at 60 and 90 kts Autorotation at 60, 90, 120 kts Frequency sweep at hover, 30, 60, 90, Vh kts 2-3-1-1 at hover, 30, 60, 90, 120 kts 2-3-1-1 in climbs and descents at 60 and 90 kts with 1000 ft/min ADS33 Accel/decel, sidestep and bob-up Hover at 5, 10, 20, 30, 40, 50 ft in turbulence behind a hangar

Table 2 summarizes the complete list of aircraft configuration and flight test data available to support the modeling efforts described in this paper. To support CFD validation and modelling research, the Bell 412 ASRA was instrumented with 256 static pressure transducers at various locations around the fuselage, engine cowls and tail boom. Rotor flapping, lead-lag and rotor strain quantities were also instrumented. These parameters are in addition to the already extensive suite of inertial, control position, air data, and engine data collected on a regular basis on this aircraft. Further information on the instrumentation and data collection flight test is available in [15].

IDENTIFICATION FRAMEWORK

Hover identified state-space model

Details and results of the identified model in hover can be found in [8]. The hover model was identified using the CIFER® frequency response method [9]. For this flight condition, only one piloted sweep for each control input were available in the Bell 412 database and the sweeps were generally focused at low and mid-frequency. Multiple 2311s records were also available and were concatenated to provided good coherence at mid/higher frequencies, as described in [8]. The combined database provides an acceptable basis for state-space system ID using CIFER® [9]. Each frequency response was determined in CIFER® and examined to determine the frequency range over which the coherence was satisfactory (e.g., all frequencies, low/mid frequency, high-frequency). Then, in the state space model structure, two outputs for each measurement (each one covering a different frequency range) were included in the identification model. The identified hover model included the coning and dynamic inflow degrees-of-freedom but after analysis, a 6-DoF quasi-steady model was found to adequately characterize the pitch, roll, yaw and heave dynamics in hover for the current study. The equations for a 6-DoF model as follows :

$$
\begin{aligned}
\dot{u} &= X_u u + X_v v + X_w w + X_p p + \left(X_q - w_0\right) q \\
&\quad + (X_r + v_0) r - g \cos\theta_0 \theta \\
&\quad + X_{\delta_{lon}} \delta_{lon} + X_{\delta_{lat}} \delta_{lat} \\
&\quad + X_{\delta_{col}} \delta_{col} + X_{\delta_{ped}} \delta_{ped} \\
\dot{v} &= Y_u u + Y_v v + Y_w w + (Y_p + w_0) p + Y_q q \\
&\quad + \ (Y_r - u_0) r \\
&\quad + g \cos\phi_0 \cos\theta_0 \phi \\
&\quad - g \sin\phi_0 \sin\theta_0 \theta \quad + Y_{\delta_{lon}} \delta_{lon} \\
&\quad + Y_{\delta_{lat}} \delta_{lat} + Y_{\delta_{col}} \delta_{col} \\
&\quad + Y_{\delta_{ped}} \delta_{ped} \\
\dot{w} &= Z_u u + Z_v v + Z_w w + (Z_p - v_0) p \\
&\quad + (Z_q + u_0) q + Z_r r \\
&\quad - g \sin\phi_0 \cos\theta_0 \phi \\
&\quad - g \cos\phi_0 \sin\theta_0 \theta \\
&\quad + Z_{\delta_{lon}} \delta_{lon} + Z_{\delta_{lat}} \delta_{lat} \\
&\quad + Z_{\delta_{col}} \delta_{col} + Z_{\delta_{ped}} \delta_{ped}
\end{aligned}
\tag{1}
$$

$$\dot{p} = L_u u + L_v v + L_w w + L_p p + L_q q + L_r r + L_{\delta_{lon}}\delta_{lon} + L_{\delta_{lat}}\delta_{lat} + L_{\delta_{col}}\delta_{col} + L_{\delta_{ped}}\delta_{ped}$$

$$\dot{q} = M_u u + M_v v + M_w w + M_p p + M_q q + M_r r + M_{\delta_{lon}}\delta_{lon} + M_{\delta_{lat}}\delta_{lat} + M_{\delta_{col}}\delta_{col} + M_{\delta_{ped}}\delta_{ped}$$

$$\dot{r} = N_u u + N_v v + N_w w + N_p p + N_q q + N_r r + N_{\delta_{lon}}\delta_{lon} + N_{\delta_{lat}}\delta_{lat} + N_{\delta_{col}}\delta_{col} + N_{\delta_{ped}}\delta_{ped}$$

Table 3 gives the pitch and roll final identified parameters, CR Bound [%] and Insensitivity [%]. It should be noticed that consistent with the guidelines from [14, pg. 396] nearly all CR are 20% or less, with only a few larger than these guidelines. From [14, pg. 361] by assuming no additional delay between flight control inputs and surfaces, it can be found that equivalent time delays τ_{lon} and τ_{lat} are dominated by the rotor time constant τ_f. By taking the average value of τ_{lon} and τ_{lat}, the rotor flap lag can be approximated as $\tau_f \cong$ 0.061. Finally, from [14, pg. 364], if we use $\tau_f \ll |1/L_p|$ with $L_p = -2.36$, it can be assumed the 6-Dof model structure assumption is adequate to represent the behavior.

MODELING FRAMEWORK

Blade-element rotor models for rotorcraft dynamics are usually used to meet the fidelity requirements for the Level-D training simulator classification. Physics-based models such as the blade element rotor models have some major advantages compared to their strictly parametric counterparts, because of their predictability and the extension of flight envelope. In addition of providing full continuous envelope and accurate performance & handling qualities, SME pilots should be able to assess special aerodynamics effects in training simulator: vortex ring state, retreating blade stall, loss of tail rotor effectiveness, engine malfunction, autorotation, icing, etc…

Baseline OO-BERM : Structure Selection

For this study, a generic OO-BERM is set-up to simulate a medium twin-engine helicopter. Four (4) rigid blades with flap and lag degrees of freedom are simulated. The anti-torque tail rotor is modeled as an actuator disc based on Bailey's equations [16]. Generic blade, fuselage, horizontal stabilizer, vertical fin and blade coefficients are used. Using the data and measurement provided in the Bell 412 ASRA data package, several parameters are fixed in the simulation: main rotor configuration (diameter, mass of blade, rotation speed) and flight control gearing (blade angles [deg] vs control inputs [%]). All aerodynamics surfaces and position are approximated using the provided drawings. Simplified flight control gearing model is used and there is no delay between control input and blade deflection. Finally, the OO-BERM is set up to use a quasi-steady inflow model which includes three inflow states representing the average and the first harmonic induced velocities over the rotor plane in the hub-wind frame.

Using small perturbation finite differences, stability and control derivatives are calculated for the Baseline OO-BERM configuration. As can be seen in Table 4, control derivatives show relative errors > 10% and static/dynamic derivatives relative errors are > 88%. It should be noted that control derivatives $L_{\delta_{lat}}$, $L_{\delta_{lon}}$ and $M_{\delta_{lon}}$ have a lower magnitude value than the CIFER® identified derivatives and on-axis dynamics derivatives L_p and M_q have higher magnitude. This results in a Baseline simulation being under-responsive to cyclic control inputs and exhibiting an overdamped response to any pilot control or atmospheric perturbation.

Table 3 CIFER® identified rolling and pitching derivatives from flight test

Par	CIFER® Value	CR (%)	Insen (%)
L_u	.0311	6.3	1.2
L_v	-.0216	10.8	2.1
L_w	0^a	-	-
L_p	-2.362	4.0	0.7
L_q	-.274	27.0	7.0
L_r	0^a	-	-
M_u	.017	8.7	1.0
M_v	.0178	8.0	1.3
M_w	0^a	-	-
M_p	-.446	6.3	1.5
M_q	-.528	11.0	2.2
M_r	0^a	-	-
$L_{\delta_{lon}}$	.023	3.8	1.5
$L_{\delta_{lat}}$	.131	2.7	0.6
$L_{\delta_{col}}$	0^a	-	-
$L_{\delta_{ped}}$	-.017	4.0	1.8
$M_{\delta_{lon}}$	.032	2.5	0.8
$M_{\delta_{lat}}$	.006	17.6	4.8
$M_{\delta_{col}}$	0^a	-	-
$M_{\delta_{ped}}$	0^a	-	-
τ_{lon}	.054	8.4	3.7
τ_{lat}	.068	6.0	2.5
τ_{lon}	.021	14.9	7.4
τ_{lon}	.084	8.7	4.2

(u, v, w in ft/s, p, q, r in rad/s, controls in %, ^{a}eliminated during model structure reduction)

Updated OO-BERM : Parameters Optimization and Adjustment of F/M increments

The first step of the OO-BERM model optimization process is to use Method 5 (Table 1) to adjust well-established theoretical physical relationships of uncertain parameters of

Table 4 CIFER® identified derivatives compared with Baseline and Updated OO-BERM calculated derivatives for hover model

Par	CIFER® Value	Baseline OO-BERM	Rel. error [%]	Updated OO-BERM	Rel. error [%]
L_u	.0311	.0028	91.00	.021	32.48
L_v	-.0216	-.1	362.96	-.032	48.15
L_w	0^a	-.002	-	-.0035	-
L_p	-2.362	-5.28	123.54	-2.35	0.51
L_q	-.274	.05	118.25	-.28	2.19
L_r	0^a	.23	-	.05	-
M_u	.017	.002	88.24	.019	11.76
M_v	.0178	.0005	97.19	.0126	29.21
M_w	0^a	-.0011	-	-.001	-
M_p	-.446	-1.6	258.74	-.43	3.59
M_q	-.528	-1.97	273.11	-.53	0.38
M_r	0^a	-.037	-	.05	-
$L_{\delta_{lon}}$	**.023**	**.0144**	**37.39**	**.021**	**8.70**
$L_{\delta_{lat}}$	**.131**	**.1144**	**12.67**	**.129**	**1.53**
$L_{\delta_{col}}$	0^a	-.01	-	-.007	-
$L_{\delta_{ped}}$	-.017	-.01	41.18	-.01	41.18
$M_{\delta_{lon}}$	**.032**	**.02856**	**10.75**	**.0323**	**0.94**
$M_{\delta_{lat}}$	**.006**	**-.00208**	**134.67**	**-.0024**	**140**
$M_{\delta_{col}}$	0^a	-.0032	-	-.003	-
$M_{\delta_{ped}}$	0^a	.0003	-	.0003	-
τ_{lon}	.054	0	100	0	100
τ_{lat}	.068	0	100	0	100
τ_{lon}	.021	0	100	0	100
τ_{lon}	.084	0	100	0	100

(u, v, w in ft/s, p, q, r in rad/s, controls in %, ^{a}eliminated during model structure reduction, **bold** used in objective function for aeromechanical parameters optimization)

the main rotor to obtain correct control derivatives. Using the algorithm presented in [7], the following rotor design parameters are treated as unknown in the optimization problem : swashplate phase angle offset $\Delta\theta_1$ [deg], rotor blade pitch-flap coupling angle δ_3 [deg] and flap hinge offset e_β[%]. The objective function J to minimize is defined as a weighted sum of the squared normalized errors of on- and off-axis pitch and roll control derivatives as :

$$\Phi \equiv \left[\Delta\theta_1, \delta_3, e_\beta\right]$$

$$\min J(\Phi) \sum_{i=1}^{4} w_i \left(1 - \frac{g_i^M(\Phi)}{g_i^S}\right)^2 \quad (2)$$

subject to the physical constraints:

$$\begin{aligned} 0^o \le \Delta\theta_1 \le 30^o \\ -30^o \le \delta_3 \le 0^o \\ 0\% < e_\beta \le 20^o \end{aligned} \quad (3)$$

where g_i^S are the identified control derivatives ($g_1^S = L_{\delta_{lon}}$, $g_2^S = L_{\delta_{lat}}$, $g_3^S = M_{\delta_{lon}}$, $g_4^S = M_{\delta_{lat}}$) and w_i are weighting factors. The OO-BERM control derivatives $g_i^M(\Phi)$ are calculated using small control perturbation finite differences for pre-defined constrained combination of design variables Φ. The measured aeromechanical parameters and the updated (optimal) solution are presented in Table 5. The Updated solution show relatively close aeromechanical parameters compared to its associated measured value. Final calculated control derivatives results (controls in %) are presented in Table 4. The updated aeromechanical parameters values found by optimization are consistent with what could be expected based on CAE empirical experience, namely:

- Increasing the flap hinge offset e_β has the effect of increasing the on-axis control derivatives ($L_{\delta_{lat}}$ and $M_{\delta_{lon}}$) of the helicopter. Since the Baseline model had lower on-axis derivatives than what was identified by CIFER®, it is to be expected that the optimal value of e_β has increased.
- Increasing the swashplate phase angle offset $\Delta\theta_1$ has the effect of increasing the off-axis control derivatives of the helicopter ($M_{\delta_{lat}}$ and $L_{\delta_{lon}}$), Since the Baseline model had lower on-axis derivatives than what was identified by CIFER®, it is to be expected that the optimal value of $\Delta\theta_1$ has increased.

The pitch-flap coupling δ_3 of the Baseline model was assumed with an initial value of zero (Table 5), this parameter has some influence on all the control derivatives. Optimizing the pitch-flap coupling allowed the solution for the hinge offset and the phase angle offset to converge closer to their physical values. Any vehicle simulation model is an approximation based on a limited number of parameters, it is therefore normal that the solution for these parameters is not equal to their measured value.

Table 5 Measured aeromechanical parameters optimal solution

	$\Delta\theta_1$[deg]	δ_3 [deg]	e_β[%]
Measured/Baseline	13	unknown/0	8
Optimal/Updated Solution	15.4	-7.3	10.3
Rel. error [%]	18.4	N/A	28.8

During early experiments of the optimization, all weighting factor w_i were set to w_i=1, but a lower weight (w_4=0.2) was required to be assigned to $g_4^S(M_{\delta_{lat}})$ to prevent

it from driving the other derivatives away from their optimal values. From Table 3, it can be seen that the relative errors are less than 9% for $L_{\delta_{lon}}$, $L_{\delta_{lat}}$, $M_{\delta_{lon}}$, except for $M_{\delta_{lat}}$ (140%), which had been purposely de-weighted. From CIFER®, it can be found that $M_{\delta_{lat}}$ has a higher CR (17.6%) and Insensitivity (4.8%) than the other control derivative. It seems that the final weighting factors w_i values are a close approximation of 1/CR, since the Cramer-Rao bound of $M_{\delta_{lat}}$ (CR = 17.6) is about 5 times higher than the other control derivatives ($L_{\delta_{lat}}$ (CR = 2.7) , $L_{\delta_{lon}}$ (CR = 3.8), and $M_{\delta_{lon}}$ (CR = 2.5)). A good practice would be to use 1/CR as initial weighting factors w_i. Finally, magnitude of $M_{\delta_{lat}}$ is much lower than the other control derivatives (4 times lower than the corresponding coupling derivative $L_{\delta_{lon}}$), which means that it has much less impact on the dynamics of the B412 ASRA.

Once the control derivatives have been updated using parameters adjustment methods, the dynamic derivatives are implemented in the OO-BERM using body aerodynamic coefficients and interactional aero parameters. Increments of forces and moments are calculated to match the dynamics derivatives ($L_p, M_p,$ etc ...). This corresponds to Method 3 (Table 1) in the list of methods defined in the NATO workgroup. In order to match the Level-D requirements for the low-speed trimmed attitude and control positions conditions (FAA [1, Table D2A] and EASA [2, SUBPART C]), trims and changes of control and attitude each side of the trim condition ($\Delta u, \Delta v$) are calculated to match the trim flight test data points. By solving equations (1) for the speed derivatives by imposing accelerations to be zero for all changes of trim condition, it is possible to find [8,19]:

$$L_u = -\left[L_{\delta_{lon}} \frac{\Delta\delta_{lon}}{\Delta u}\right] ; \quad M_u = -\left[M_{\delta_{lon}} \frac{\Delta\delta_{lon}}{\Delta u}\right]$$

$$L_v = -\left[L_{\delta_{lat}} \frac{\Delta\delta_{lat}}{\Delta v} + L_{\delta_{lon}} \frac{\Delta\delta_{lon}}{\Delta v} + L_{\delta_{ped}} \frac{\Delta\delta_{ped}}{\Delta v}\right] \quad (4)$$

$$M_v = -\left[M_{\delta_{lat}} \frac{\Delta\delta_{lat}}{\Delta v} + M_{\delta_{lon}} \frac{\Delta\delta_{lon}}{\Delta v} + M_{\delta_{ped}} \frac{\Delta\delta_{ped}}{\Delta v}\right]$$

where only the control gradient contributions are retained. Linear regressions on the control and attitude gradients are done using the runs up, down, left and right runway trims maneuvers included in the Bell 412 ASRA database. Due to lack of available data (vertical climb/descent in hover), it should be noted that changes of control and attitude on each side of the trim condition in function of Δw were set 0, except $\frac{\Delta\delta_{col}}{\Delta w}$. Table 6 show linear regression value results. Results of the calculated updated OO-BERM speed derivatives ($L_u, M_u,$ etc…). are shown in Table 4.

OO-BERM Model Validation

Validation is done first in the frequency domain to compare on- and off-axis responses. Figure 3 shows frequency domain comparison of the Baseline/Updated OO-BERM models with the flight test data and the identified hover model using CIFER. As expected from the Baseline OO-BERM calculated derivatives in Table 4, Baseline OO-BERM frequency response show poor results compared to the flight test data. The significant control derivatives are too low ($L_{\delta_{lon}}, L_{\delta_{lat}}$ and $M_{\delta_{lon}}$), the on axis damping terms (L_p, M_q) are too high and almost all the other static and dynamic terms have large errors.

Table 6 Trim control gradients with respect to airspeed in hover

Par	Value		Value		Value
$\frac{\Delta\delta_{lon}}{\Delta u}$	-0.44	$\frac{\Delta\delta_{lon}}{\Delta v}$	-0.369	$\frac{\Delta\delta_{lon}}{\Delta w}$	0^b
$\frac{\Delta\delta_{lat}}{\Delta u}$	0^a	$\frac{\Delta\delta_{lat}}{\Delta v}$	0.294	$\frac{\Delta\delta_{lat}}{\Delta w}$	0^b
$\frac{\Delta\delta_{dir}}{\Delta u}$	0^a	$\frac{\Delta\delta_{dir}}{\Delta v}$	-0.344	$\frac{\Delta\delta_{dir}}{\Delta w}$	0^b
$\frac{\Delta\delta_{col}}{\Delta u}$	0^a	$\frac{\Delta\delta_{col}}{\Delta v}$	0^a	$\frac{\Delta\delta_{col}}{\Delta w}$	-0.5^b
$\frac{\Delta\phi}{\Delta u}$	0^a	$\frac{\Delta\phi}{\Delta v}$	0.1829	$\frac{\Delta\phi}{\Delta w}$	0^b
$\frac{\Delta\theta}{\Delta u}$	0.102^a	$\frac{\Delta\theta}{\Delta v}$	0^a	$\frac{\Delta\theta}{\Delta w}$	0^b

(u, v, w in ft/s, controls in %, [a]: eliminated, [b]: imposed in Baseline configuration)

Figure 3 shows good results for the Updated OO-BERM model compared to the measurements and the identified linear model from CIFER®. Indeed, for on and off axis pitch and roll frequency domain responses were the coherence is acceptable (> 0.6). p/δ_{lat}, p/δ_{lon} and q/δ_{lon} responses show good match for both magnitude and phase, with the Updated OO-BERM model frequency responses having a difference of phase of 20 degrees at 10 rad/s compared to the Model CIFER® frequency responses. Off axis response q/δ_{lat} show an average maximum offset of 3.3 dB and a drift in the phase. This is consistent with the error still present for $M_{\delta_{lat}}$ in the updated model (Table 4). This means that the parameters $\Delta\theta_1, \delta_3$ and e_β were not sufficient to match all the control derivatives and another design variable affecting $M_{\delta_{lat}}$would be required. However, as mentioned in the previous section, an error in $M_{\delta_{lat}}$ may not have a significant impact on the overall dynamics of the helicopter.

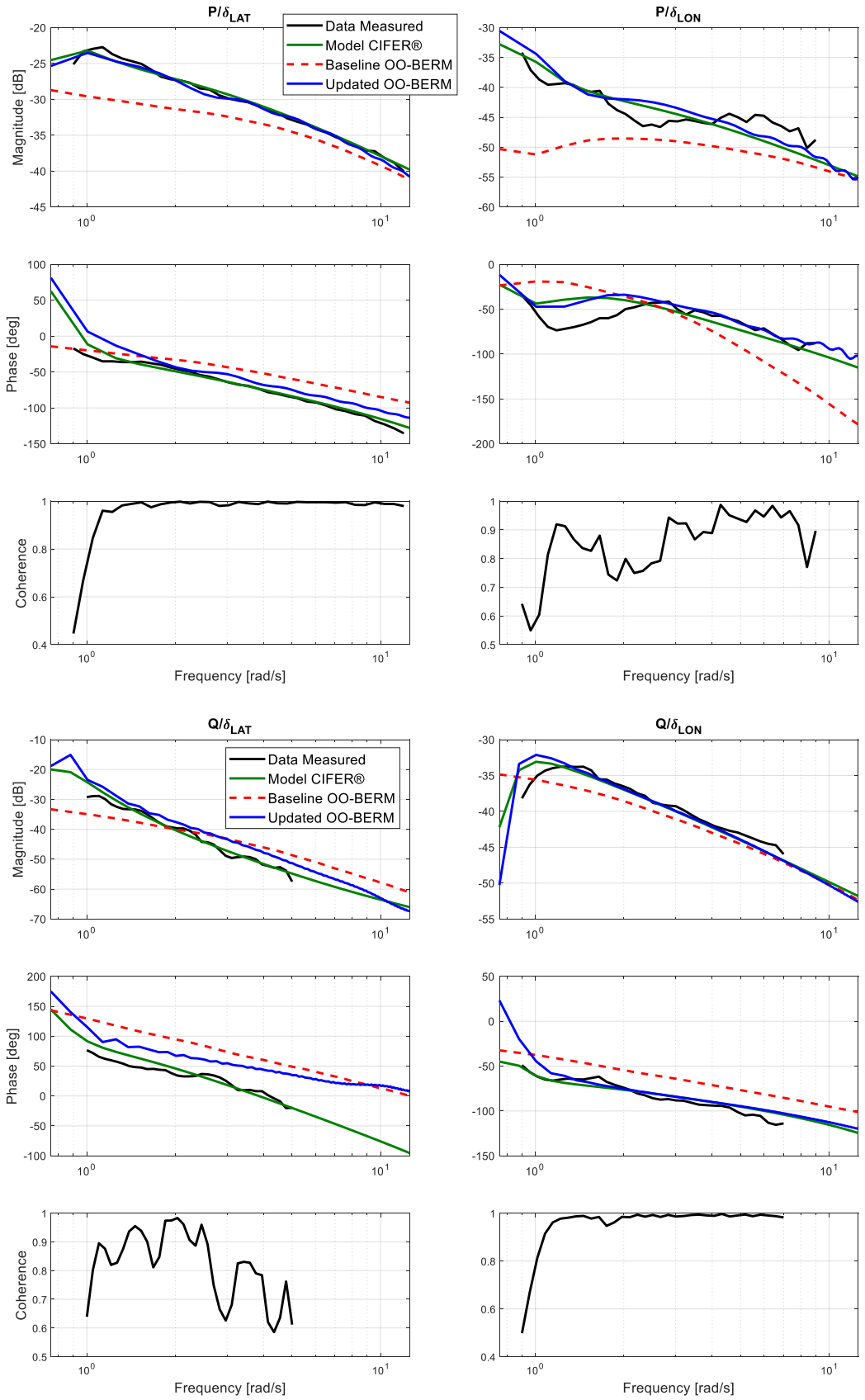

Figure 3 Frequency domain comparison of the flight data with identified CIFER® hover model and Baseline/Updated OO-BERM model (top: roll rate, bottom: pitch rate)

The FAA "14 CFR Part 60" [1] standard in America and the EASA "CS-FSTD(H) Initial Issue" [2] standard in Europe formalize the qualifying criteria and procedures needed for approval for each of the major components of a Level-D helicopter simulator. They both use a functional performance standard called Qualification Test Guide (QTG). The QTG is a document designed to assess and validate that performance and handling qualities of a simulator agree within prescribed limits with those of the aircraft and that all applicable regulatory requirements have been met. The QTG includes both the helicopter flight test data and simulator data used to support the validation. A flight test data package must contain more than one hundred individual events to meet the minimum Level-D validation requirements. The qualifying criteria of the mathematical model's performance loop are formulated by using 'tolerances' and it includes an evaluation based on the comparison between reference flight tests data and results of identical tests computed on a simulator. Also, subjective validation requirements comprise a series of training tasks and abnormal conditions that are normally rigorously assessed during the final qualification to ensure there are no discontinuities between all simulated fight regimes. The combination of objective and subjective testing is meant to guarantee that the fully integrated simulator is sufficiently representative of the aircraft. A complete background and history on the qualification of helicopter training simulators over the years can be found here [20].

In hover, both FAA [1, Table D2A] and EASA [2, SUBPART C] requires for longitudinal cyclic input cases a tolerance of ±10% or 2 deg/sec (whichever is the highest) on the pitch rate response (q) and of ±1.5 degrees on the pitch attitude change ($\Delta\theta$) following a control input. For lateral cyclic input cases, a tolerance of ±10% or 3 deg/sec (whichever is the highest) on the roll rate response (p) and of ±3 degrees on the roll attitude change ($\Delta\phi$) following a control input are required. Also, all off-axis parameters need to follow the correct trend and have the correct magnitude. Initial condition tuning is requried for both validation cases to be within QTG tolerances for the updated OO-BERM. It should be noted that the same initial conditions were applied for each case for the Baseline and updated OO-BERM. The initial condition tunning is required because the flight test data is never perfectly trimmed and small initial linear and angular accelerations are usually required when starting the simulation run on a maneuver to ensure that the simulation result is in a steady state before the control inputs.

Figure 4 shows time domain validation for longitudinal and lateral cyclic input cases of the Baseline and Updated OO-BERM. Grey bands represents the allowable tolerance band. By looking at both frequency responses (Figure 3) and time responses (Figure 4), the Baseline OO-BERM responses are overly damped for the rolling and pitching moments following a pitch input. Roll response due to lateral input is overdamped and pitch response does not follow the trend well.

Finally, from Figure 4, one can conclude that the Updated OO-BERM simulation time domain responses are within the FAA and EASA tolerance bands for the on-axis control input and has a correct trend and magnitude for off-axis responses within 2x the tolerance bands.

QUANTITATIVE METRIC FIDELITY

In the frequency domain, the boundaries for the allowable mismatch are called Maximum Unnoticeable Added Dynamics (MUAD) envelops. They were first proposed by Hodgkinson [17] to assess lower order model model accuracy for fixed-wing handling-qualities applications. Being within the MUADs boundaries means that the model mismatch error will remain unnoticed to a SME pilot and therefore the added dynamics is acceptable. The same analysis approach was first proposed by Tischler [21, pp 52-54] for model fidelity assessment.

By looking at Figure 5, one can see that the shape of MUAD envelopes is like an hourglass. Pilots are more sensitive to the added dynamics at mid-frequencies (around 1-3 rad/sec), which are characteristic of the pilot operating frequencies. As a result, the MUAD allowable mismatch boundaries are most narrow in the range. At either end of the envelopes, their shape becomes wider. This means that beyond and below these frequencies pilots are less sensitive to the added dynamics.

The most important characteristic of MUADs envelopes is that the boundaries are defined by a perceived change in the handling qualities. Mitchell et al. [18] proposed an experiment to study the pilot sensitivity on the variations in the helicopter dynamics. Instead of determining the critical added dynamics by degrading handling qualities, the boundaries were found by SME pilots' rating the noticeability of the added dynamics in the so-called Allowable Error Envelops (AEE). The boundaries on MUAD show the envelopes based on handling quality, the AEE boundaries show the envelopes based on pilot's opinion on the task performance. Figure 5 show the AEE/MUAD bounds for the OO-BERM compared to flight test data. Also, QTG tolerance bands in the frequency domain were added in for each axis responses:

$$|QTG_{band}(j\omega)|_{dB} = \pm 20\log_{10}(\max(abs, rel)) \qquad \angle QTG_{band}(j\omega) = \pm\Delta t\frac{\omega}{2\pi} * 360 \text{ deg} \tag{5}$$

where $|...|_{dB}$ is the QTG magnitude tolerance band, $\angle(...)$ is the QTG phase tolerance band, *abs* is the absolute QTG tolerance band, *rel* is the QTG relative tolerance band and Δt is the delay introduced by the simulation. It should be noted that the magnitude tolerance is constant for every frequency (gain), whereas the phase tolerance will increase with the frequency.

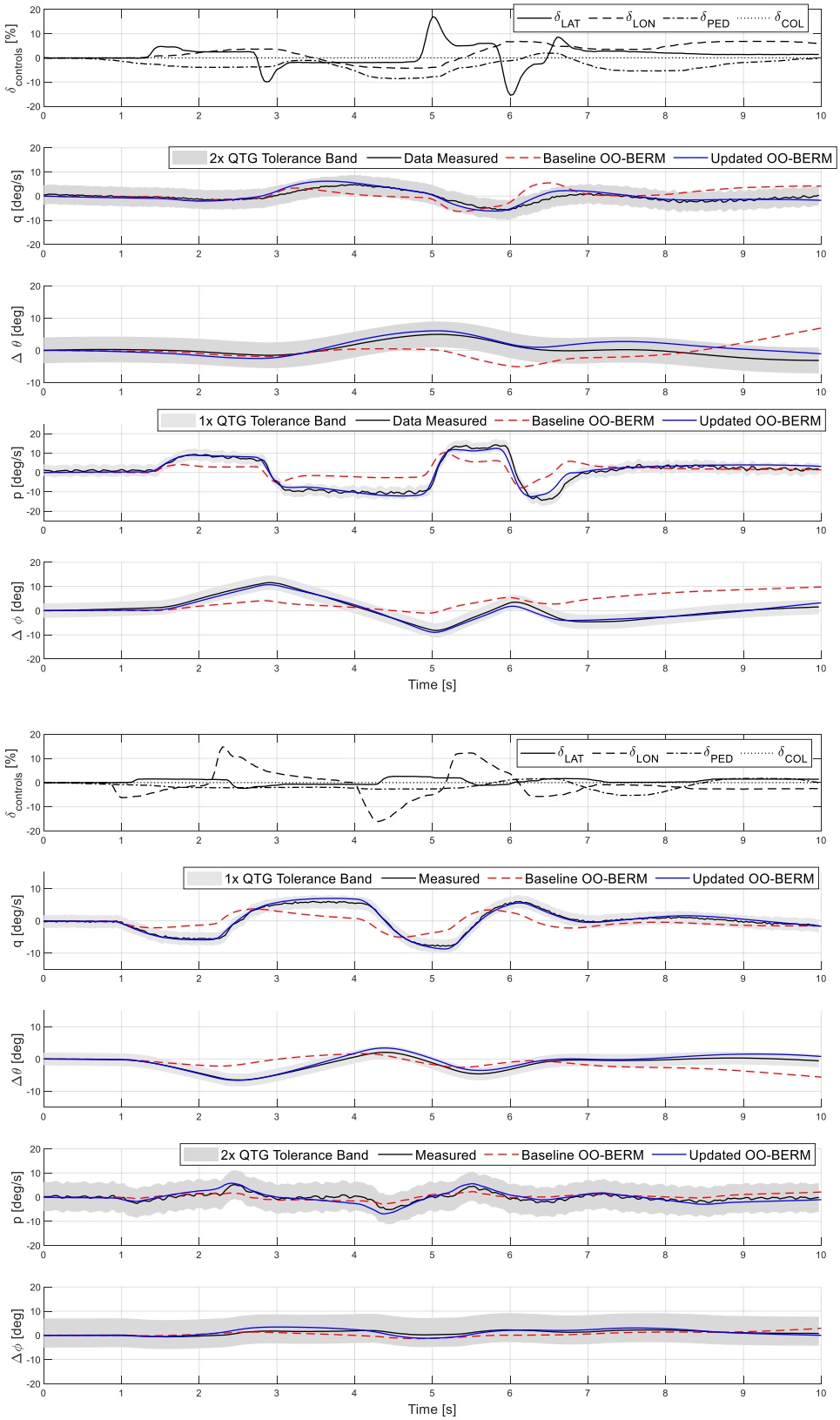

Figure 4 Time domain validation of the hover model OO-BERM against flight data (top: lateral cyclic input, bottom: longitudinal cyclic input)

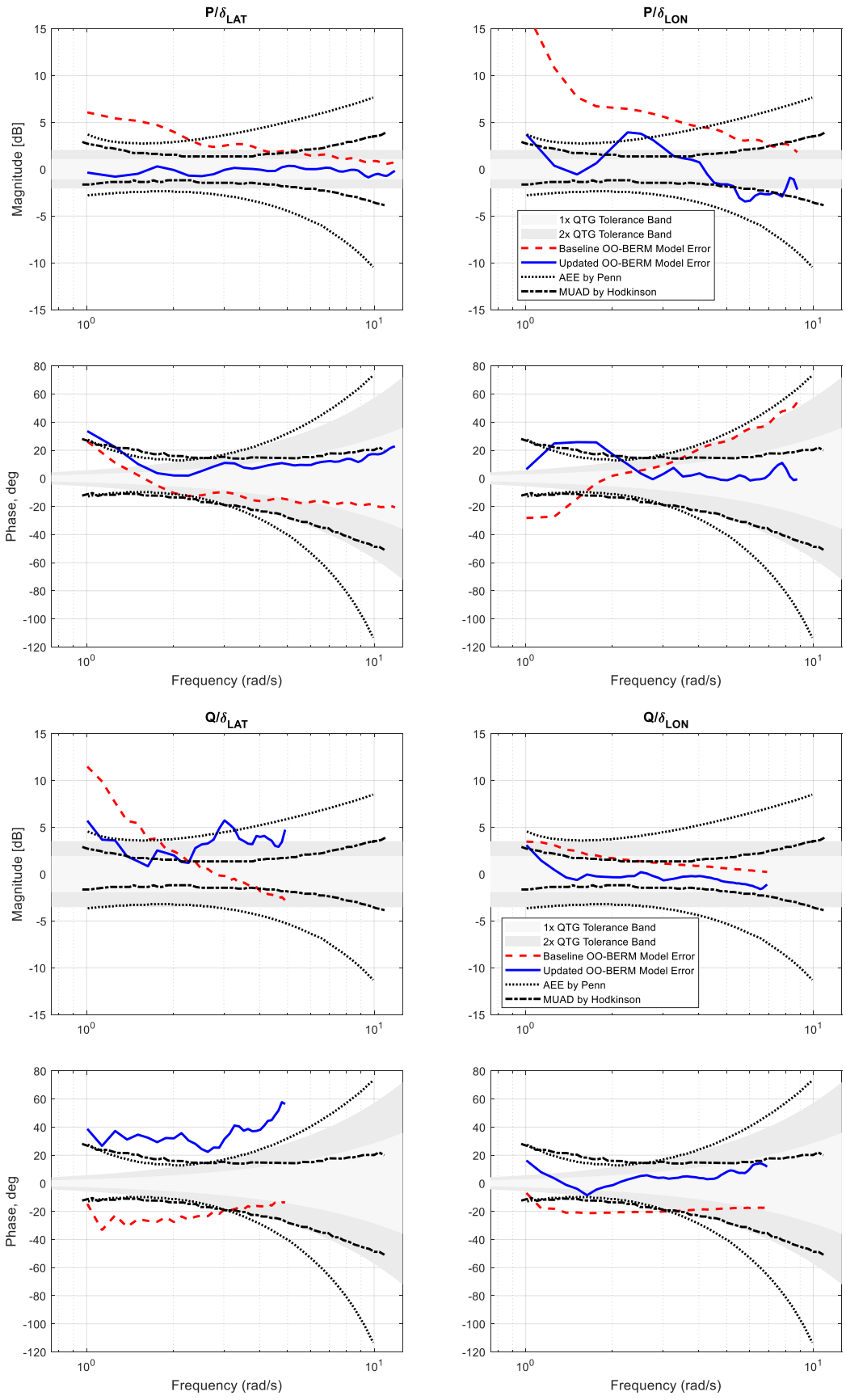

Figure 5 AEE/MUAD/QTG bounds and model error (top: roll rate, bottom: pitch rate)

Both FAA [1, Paragraph 15] and EASA [2, Appendix 5] define the maximum permissible delay to be 100 ms. This delay can be measured through the 'Transport delay' test. 'Transport delay' defines the total training simulator system processing time required for an input signal from a pilot primary flight control until the motion system, visual system, or instrument response. It is the overall time delay incurred from signal input until output response perceptible by the pilots. In the case where only the vehicle dynamics loop is analyzed (flight dynamics, flight controls, engines and autopilot), it is reasonable to reduce this maximum delay to 50 ms.

In Figure 6, the sequence to measure the transport delay from control inputs through the interface is shown. In a typical training simulator configuration, there will be up to one iteration between flight controls input and the simulator flight control interface, which calculates the main rotor blades angles from the flight control measured position. This is because a flight controls input can occur at any time in the iteration, but it will not be processed before the start of the new iteration. There is at least one iteration between the simulator flight control interface and the Host where helicopter aerodynamics is calculated and integrated. This adds up to up to 2 iteration delays that are completely independent from the model itself. If a training simulator is running at 60 Hz, 3 iterations will mean a reasonable delay of 50 ms while allowing for a very small model error in in term of delay.

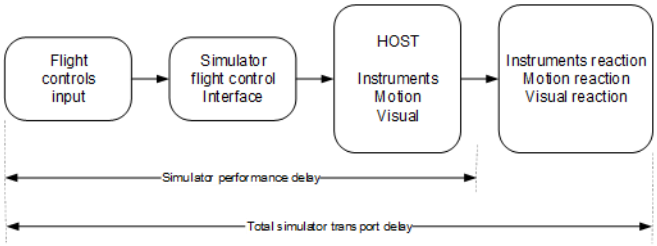

Figure 6 Transport Delay for training simulator

Finally, in Figure 5, the Model Error is determined from:

(6) Model Error = OO-BERM response / flight test response

As can be seen in Figure 5, the MUAD boundaries are consistent with the QTG boundaries, especially at mid frequencies, allowing both fidelity assessment methods to be used with a common implied level of fidelity. When comparing the QTG tolerance band to the MUAD, in figure 6, it can be seen that the magnitude QTG tolerance band is more restrictive at lower and higher frequency. The phase tolerance of the QTG band is very restrictive at lower frequency when compared to the MUAD boundary. If we assume that the MUAD boundaries are correct, it may indicate that the QTG criterions are sometimes more restrictive than what a pilot would notice at very low and high frequencies. From Figure 5, the Updated OO-BERM frequency domain errors are within the FAA and EASA tolerance bands for the on-axis responses and off-axis responses are reasonably within 2x the tolerance bands. As expected, the Baseline OO-BERM frequency domain errors show poor results. From Figure 4, off-axis roll time response to longitudinal cyclic input seems to show reasonnable behavior, but when we look at p/δ_{lon} OO-BERM frequency domain error from Figure 5, is not within the MUAD & QTG boundaries throughout the whole range of frequencies. Similar observation can be applied to off-axis pitch time response to lateral cyclic input q/δ_{lat}.

Finally, two other metrics that are widely used in the piloted simulator community [8, 9, 12] are calculated for comparison purpose, namely the frequency domain integrated cost metric J and the mismatch mean square cost function J_{rms}.

From [9, pg 389], it can be found that the frequency response matrix of a linear state-space system, like the 6-DoF quasi-steady model problem of eq (1), is determined as

(7) $$T(s) = C(sI - A)^{-1}B + D$$

where I is the identity matrix. The cost function J to be minimized for the frequency response method is

(8) $$J = \frac{20}{N_\omega}\sum_{k=1}^{N_\omega} w_\gamma(\omega_k)\left[(|T_m(\omega_k)|_{dB} - |T(\omega_k)|_{dB})^2 + w_{ap}(\angle T_m(\omega_k) - \angle T(\omega_k))^2\right]$$

where T and T_m are a unique frequency response and its measured counterpart. N_ω is the number of frequency points in the frequency interval $[\omega_1, \omega_{N_\omega}]$. $|\ldots|_{dB}$ denotes the amplitude in dB and $\angle(\ldots)$ the phase angle in deg. w_γ is an optional weighting function based on the coherence γ between the input and the output at each frequency. w_γ is defined as [8] :

(9) $$w_\gamma(\omega_k) = \left[1.58\left(1 - e^{\gamma^2_{xy}(\omega_k)}\right)\right]^2$$

Coherence weighting w_γ is used to de-weight unreliable flight data and the minimum acceptable coherence γ = 0.6 is used to limit the frequency range. w_{ap} in Eq. (8) is the relative weighting between amplitude and phase errors, with a default value of $w_{ap} = 0.01745$. From [9, pg 389], it is found that the acceptable standard value for model fidelity is $J_{ave} < 100$. It should be noted that J_{ave} is the average cost of all frequency responses. Table 7 show the frequency domain integrated cost of p/δ_{lat}, p/δ_{lon}, q/δ_{lat} and q/δ_{lon}. As expected from previous results, Baseline OO-BERM results for on- ($J > 250$) and off-axis ($J > 400$) show poor frequency domain integrated cost compared to the Updated OO-BERM, where the on-axis frequency responses p/δ_{lat} and q/δ_{lon} are below the acceptable standard ($J < 65$). Off-axis response cost p/δ_{lon} is reasonably low ($J = 118.9$),

whereas q/δ_{lat} has a very high cost ($J = 518.7$). From Figure 4, it can be seen that the Updated OO-BERM simulation time domain responses for the on-axis control input are in agreement with results from Table 7. Also, off-axis roll time response to longitudinal cyclic input seems to show reasonably behavior as expected. With a very high cost ($J = 518.7$), off-axis pitch time response to lateral cyclic input q/δ_{lat}, one would expect poor results, but the response is within 2x the tolerance bands.

Table 7 Frequency Domain Integrated Cost J

Freq. resp	J Baseline OO-BERM	J Updated OO-BERM
p/δ_{lat}	400.9	64.2
p/δ_{lon}	842.6	118.9
q/δ_{lat}	1111.9	518.7
q/δ_{lon}	258.6	34.5

Finally, the root mean square cost function J_{rms} error provides an overall measure of model time-domain accuracy and is defined as

$$J_{rms} = \sqrt{\frac{1}{N_t n_y}\sum_{k=1}^{N_t}(\boldsymbol{z}(t_k)-\boldsymbol{y}(t_k))^T(\boldsymbol{z}(t_k)-\boldsymbol{y}(t_k))} \quad (10)$$

with $\boldsymbol{z}$ measurement of output vector of $\boldsymbol{y}^T = [p, q, \phi, \theta]$ and data units of deg/s for the angular rates and deg for the Euler angles. Values of J_{rms} below 1.0-2.0 for rotorcraft models generally reflect acceptable levels of accuracy for flight-dynamics modeling [8]. J_{rms} value were calculated for each model using time domain validation OO-BERM against flight data input maneuvers in hover. The results are shown is Table 8. As expected from results from Figure 4, Baseline OO-BERM results both validation cases show a higher J_{rms} cost compared to the Updated OO-BERM.

Table 8 Root Mean Square Cost J_{rms}

Time domain validation	J_{rms} Baseline OO-BERM	J_{rms} Updated OO-BERM
lateral input	2.5770	0.5845
long. input	1.4944	0.4026

CONCLUSIONS

The paper presented the different steps leading to a Level-D physics-based model in hover for a Bell 412. Frequency domain system identification was performed for hover using CIFER® and results output from the OO-BERM modeling framework are shown. Validation is done in the frequency and time domain. Finally, alternative metrics assessment were presented. The results lead to the following conclusions :

- In hover, the frequency sweep and concatenated 2311 inputs are used to provide an adequate frequency response database for the identification. For the Bell 412, a quasi-steady (6DOF) model is adequate to represent the pitch and roll dynamics in hover.
- A full non-linear object-oriented blade elements rotor model (OO-BERM) was parameterized to match these stability and control derivatives.
- The helicopter control derivatives were optimized successfully by varying main rotor aeromechanical parameters such as the swashplate phase angle offset $\Delta\theta_1$ [deg], rotor blade pitch-flap coupling angle δ_3 [deg] and flap hinge offset e_β[%].
- The static and dynamic stability derivatives of the helicopter were calculated using forces and moments increment on the fuselage
- This modeling approach can be used to match both Level-D requirements (converted into a frequency domain formulation) and the alternative fidelity metrics stated above in time domain and frequency domain.
- The Level D requirements were compared to the MUAD criterion. The MUAD criterion is comparable to the tolerance bands at mid-frequencies, but less restrictive than the QTG tolerance band at higher and lower frequencies.

Future research will include additional states and more design variables in the optimization procedure.

Author contact:

Vincent Myrand-Lapierre vincent.myrandlapierre@cae.com
Mark B. Tischler
Marilena D. Pavel m.d.pavel@tudelft.nl
Michel Nadeau-Beaulieu michel.nadeaubeaulieu@cae.com
Olaf Stroosma o.stroosma@tudelft.nl
Bill Gubbels arthur.gubbels@nrc-cnrc.gc.ca
Mark White mdw@liverpool.ac.uk

ACKNOWLEDGMENTS

The authors are grateful to Alireza Razavi and Sebastien Bolduc for supporting this work.

REFERENCES

1. anon., Federal Aviation Administration, National Simulator Program, 14 CFR Part 60, 2016.
2. anon., European Aviation Safety Agency, CS-FSTD(H), Certification Specifications for Helicopter Flight Simulation Training Devices, Initial Issue, June 2012.

3. Van Esbroeck, P., and Giannias, N., "Model Development of a Level D Black Hawk Flight Simulator," Paper No. AIAA-2000-4582, AIAA Modeling and Simulation Technologies Conference, Denver, CO, August 2000.

4. Spira, D., Agnerian, A., and Boulianne, M.-A., “Validation of High Fidelity Helicopter Simulation Models: An A/MH-6M Case Study”, American Helicopter Society 62th Annual Forum, Phoenix, AZ, May 2006.

5. Spira, D., and Martelli-Garon, P., “Physics-Based Modelling of Asymmetric Control Response for Level-D Helicopter Simulation” AHS 64th Annual Forum, April 29-May 2, 2008, Montreal, Canada.

6. Theophanides, M., and Spira, D., "An Object-Oriented Framework for Blade Element Rotor Modelling and Scalable Flight Mechanics Simulation " Proceedings of the 35th European Rotorcraft Forum, Hamburg, Germany, September 22-25, 2009.

7. Spira, D., Myrand-Lapierre, V., and Soucy, O., “Reducing Blade Element Model Configuration Data Requirements Using System Identification and Optimization”, American Helicopter Society 68th Annual Forum, Fort Worth Texas, May, 2012.

8. Seher-Weiß., S., Tischler, M.B., Scepanovic, J., and Gubbels, B., “Bell 412 System Identification and Model Fidelity Assessment for Hover and Forward Flight”, 8th Asian/Australian Rotorcraft Forum, Ankara, Turkey, Oct. 30 - Nov. 2, 2019.

9. Tischler, M. B., and Remple, R. K., Aircraft and Rotorcraft System Identification: Engineering Methods with Flight Test Examples, 2nd edition, Reston, VA : American Institute of Aeronautics and Astronautics, 2012.

10. Jategaonkar, R.J., Flight Vehicle System Identification: A Time Domain Methodology, American Institute of Aeronautics and Astronautics, Reston, Virginia, 2006

11. Klein, V., and Morelli, E.A. Aircraft System Identification - Theory and Practice, AIAA Education Series, Reston, VA, August 2006.

12. Seher-Weiß. S., Greiser, S. Wartmann, J., Myrand-Lapierre, V., Gubbels, A. Ricciardi, J., and Hui, K., “Bell 412 System Identification: Comparing Methods and Tools”, Vertical Flight Society - Forum 75, Philadelphia, PA, May 13-16, 2019.

13. Seher-Weiß, S., “ACT/FHS System Identification Including Rotor and Engine Dynamics”, AHS International 73rd Annual Forum, Fort Worth, Texas, USA, May 9–11, 2017.

14. Wartmann, J. and Greiser, S., “Identification and Selection of Rotorcraft Candidate Models to Predict Handling Qualities and Dynamic Stability”, European Rotorcraft Forum, Delft, Netherlands, 2018.

15. Gubbels, A.W., Carignan, S., Ellis, K., Dillon, J., Bastian, M., Swail, C. and Wilkinson, C., “NRC Bell 412 Aircraft Fuselage Pressure and Rotor State Data Collection Flight Test”, 32nd European Rotorcraft Forum, Maastricht, Netherlands, September 12-14, 2006.

16. Bailey, F.J., "A Simplified Theoretical Method of Determining the Characteristics of a Lifting Rotor in Forward Flight," NACA Report No. 716, 1941.

17. Hodkinson, J., Aircraft Handling Qualities, AIAA Education Series, American Institute of Aeronautics and Astronautics, Reston, VA, 1998.

18. Mitchell, D.G., et. Al, Evolution, Revolution, And Challenges Of Handling Qualities, Journal Of Guidance, Control, And Dynamics, Vol. 27, No. 1, January–February 2004, pp. 12-28.

19. Tobias, E. L. and Tischler, M. B., “A Model Stitching Architecture for Continuous Full Flight-Envelope Simulation of Fixed-Wing Aircraft and Rotorcraft from Discrete-Point Linear Models,” U.S. Army AMRDEC Special Report RDMR-AF-16-01, April 2016.

20. M. D. Pavel, G. D. Padfield, G. Roth, M. Hamers, M. White, Taghizad, “Validation of Mathematical Models for Helicopter Flight Simulators Current and Future Challenges.” The Aeronautical Journal, Vol. 117, No. 1189, 2013.

21. Tischler, M. B., Advances in Aircraft Flight Control, Edited, Taylor & Francis Ltd, London, U.K., 1996.